Real-Time Path Integral Methods, Quantum Master Equations, and Classical vs. Quantum Memory

Sambarta Chatterjee and Nancy Makri*

Department of Chemistry, University of Illinois,
505 S. Mathews Avenue, Urbana, Illinois 61801

Abstract

We investigate the use of accurate path integral methods, namely the quasi-adiabatic propagator path integral (QuAPI) and the quantum-classical path integral (QCPI), for generating the memory kernel entering generalized quantum master equations (GQME). Our calculations indicate that the length of the memory kernel in system-bath models is equal to the full length of time nonlocality encoded in the Feynman-Vernon influence functional, and that the solution of the GQME with a QuAPI kernel is identical to that obtained through an iterative QuAPI calculation with the same memory length. Further, we show that the memory length in iterative QCPI calculations is always shorter than the GQME kernel memory length. This stems from the ability of the QCPI methodology to pretreat all memory effects of a classical nature (i.e. those associated with phonon absorption and stimulated emission), as well as some of the quantum memory contributions (arising from spontaneous phonon emission). Further, trajectory based iterative QCPI simulations can fully account for important structural/conformational changes that may occur on very long time scales and which cannot be captured via master equation treatments.

Corresponding author's email: nmakri@illinois.edu. Phone: 217-333-6589.

I. Introduction

Quantum mechanical effects, such as tunneling, zero-point energy and phase interference, play a crucial role in the understanding of important processes in biology, catalysis, energy harvesting and quantum computation. In recent years, theoretical efforts for developing simulation methods capable of following the dynamics of such processes with sufficient accuracy have intensified. The dissipative two-level system (TLS) (or spin-boson) model[1] continues to serve as the paradigm of tunneling in the condensed phase. The iterative quasi-adiabatic propagator path integral methodology[2-9] (QuAPI), along with its various extensions,[10-21] enables fully quantum mechanical simulation of dissipative TLS dynamics over long propagation times and without restrictions on the frequencies of the harmonic bath degrees of freedom and their coupling to the system, and other methods are also available for low temperatures[22] or for special forms of the bath spectral density.[23] By exploiting the Gaussian response approximation (which has been put on a rigorous basis through a path integral analysis[24]), a plethora of processes in complex environments have been investigated by simulating system-bath Hamiltonians.

In sharp contrast to these advances in system-bath methodology, the quantum dynamics of more complex processes continues to remain out of reach. Even the simple system-bath Hamiltonian has parameter regimes that remain challenging, especially when the system involves many quantum states. Further, while the harmonic bath mapping is justifiable in many situations, it is hard to know *a priori* whether it provides a faithful description of a particular process with sufficient chemical complexity. Thus, the development of accurate algorithms for simulating the quantum dynamics of condensed phase processes is highly desirable.

Significant progress has been made in this direction, in particular in the context of quantum-classical approximations for nonadiabatic dynamics, where a large number of degrees of freedom, which correspond to the nuclei of a solvent or biological molecule and which are assumed to follow classical dynamics, evolve on discrete Born-Oppenheimer or diabatic states that are coupled to each other. Combining quantum and classical mechanics poses severe challenges, owing to the incompatibility between local Newtonian trajectories and delocalized wavefunctions. The oldest mixed quantum-classical treatment is the Ehrenfest mean-field model,[25] which is practical and appealing, but fails to yield physically correct dynamics and product distributions. Surface hopping methods[26, 27] correct the major shortcomings of the Ehrenfest model and have been used in many investigations, although they are not capable of capturing decoherence and have been shown to lead to large error in some regimes. The Meyer-Miller (MM) mapping Hamiltonian approach[28, 29] bypasses the quantum-classical dilemma by replacing the quantum states by continuous degrees of freedom, which must then be described (along with the coordinates of the nuclei) by linearized semiclassical[30] (LSC) trajectory methods. Methods based on the mixed quantum-classical Liouville equation,[31, 32] in particular its momentum-jump formulation[33, 34] (MJ-QCLE) offers a rigorous solution, although the computational demands of the method increase exponentially with propagation time. The quantum-classical path integral[35-37] (QCPI) methodology, which corresponds to the stationary phase limit (with respect to the classical nuclei) of the path integral representation of the propagator in the space of all particles, offers a rigorous formulation which – solely through phase interference – correctly captures the decoherence induced by the classical degrees of freedom. The QCPI algorithm scales linearly with propagation time and has been shown to be practical for simulating charge transfer processes in the condensed phase[38] without *ad hoc* assumptions or adjustable parameters. Last, our group has recently developed a fully quantum mechanical modular decomposition of the path integral[39, 40] (MPI), which allows simulation of systems characterized by a quasi-one-dimensional topology with linear scaling. The MPI

formulation is ideally suited to exciton energy transfer in systems of many units, each with electronic states coupled to arbitrary numbers of vibrational or phonon modes, at zero or finite temperature.[41]

In many situations the object of interest is the reduced density matrix (RDM) of the discrete quantum system, or a time correlation function of system operators, and some formulations directly target these properties. In the path integral formulation,[42] the effects of the environment are captured through the influence functional, which can be evaluated exactly in the case of a harmonic bath (giving rise to the Feynman-Vernon expression[43]). In the QCPI methodology, a semiclassical approximation of the influence functional captures the effects of the nuclei via classical trajectories subject to forces specified by the state of the quantum system along a forward-backward path.[35] The influence functional contains nonlocal interactions, commonly referred to as memory effects, which prevent the subsequent reduction of the problem to that of a single quantum particle. Exploiting the memory-quenching effects of condensed phase environments allows an iterative tensor product decomposition of these path integral-based algorithms (i-QuAPI[5] and i-QCPI[36]), which leads to linear scaling with propagation length. Since the influence functional needs to be included along all path segments within the memory length, the crudest form of these methods scales exponentially with the number of time steps necessary to span the memory. However, dramatic savings are possible through additional decompositions[44, 45] and path filtering.[7, 8, 10, 46] Further, it has been shown that the most prominent ("classical memory") component of the influence functional is automatically accounted for in QCPI through the classical trajectories,[47] that some of the residual "quantum memory" component can also be removed,[48] and the time step can be increased,[49] thereby significantly shortening the memory length.

An alternative approach is used in quantum master equation approaches,[50, 51] which lump the effects of the environment into a two-time memory kernel. The storage requirements of these approaches are considerably lower, as they do not need to store quantum paths over several time steps. However, obtaining the kernel requires knowledge of the system dynamics under the influence of the environment over the kernel memory length. Evaluation of the kernel using perturbation theory and the Markovian approximation leads to the well-known Bloch-Redfield equations.[52] In the absence of such assumptions, Geva and coworkers have shown that the kernel in the Nakajima-Zwanzig generalized quantum master equation[50, 51] (GQME) can be obtained from time correlation functions.[53] Recent work based on either the Nakajima-Zwanzig or the Mori formalism[54] has demonstrated that the kernel may be obtained from knowledge of the RDM for all possible initial conditions.[55-58] Thus, if one could reliably obtain the GQME kernel over its memory length, solution the GQME would yield the RDM dynamics over longer times.

Several approximate methods have been investigated toward this goal, including Ehrenfest dynamics,[59, 60] LSC approximations to the MM mapping Hamiltonian,[58] and truncated MJ-QCLE methods.[61] These methods were found to reproduce the true GQME kernel reasonably well for some spin-boson models, while the resulting GQME dynamics was very good in some regimes. The key to the success of these approaches may lie in the relatively weak coupling and short memory length of these models, which allows approximate methods to yield relatively good results, since errors tend to grow with increasing propagation time. Still, it is not possible to know the accuracy of GQME results with approximate kernels unless numerically exact results for the system of interest are available.

An intriguing possibility is to compute the GQME kernel using methods capable of producing numerically exact or at least highly accurate results. In some cases of interest, real-time path integral Monte Carlo methods can be converged over the time span of the memory kernel.[62, 63] In the case of system-bath Hamiltonians, numerically exact kernel calculations have been reported based on the correlation function approach in conjunction with QuAPI calculations,[53] and also with the RDM approach using the

multiconfiguration time-dependent Hartree methodology.[57] In addition to full-path (non-iterative) QuAPI calculations, numerically exact results on system bath Hamiltonians may also be obtained using QCPI (which is also exact for a system coupled to a harmonic bath). While both QuAPI and QCPI can produce long-time dynamics, with effort that scales linearly with propagation time, the GQME array storage requirements are considerably more modest. It is thus important to assess the advantages and drawbacks of the GQME with path integral-generated kernels, and to compare the effort required for obtaining the exact long-time dynamics of a system-bath Hamiltonian via i-QuAPI, i-QCPI, or the GQME approach. A key question in this regard is the memory length required for convergence of the GQME, compared to the memory required in each of the two path integral-based methods. While various conjectures have been discussed, it appears that no consensus has been reached on this question.[53, 55] Further, in the case of a complex anharmonic environment, it appears that QCPI offers the most rigorous and robust formulation that converges with relatively modest effort in several regimes of interest, thus it may be the best candidate for computing the memory kernel for use in the GQME.

In this paper we address these questions by performing QuAPI and QCPI calculations to generate the GQME kernel and solving the GQME equation to obtain long-time dynamics on dissipative TLSs in several parameter regimes. We also compare the relevant memory lengths, i.e., the Feynman-Vernon influence functional memory that enters the i-QuAPI formulation, the quantum memory length entering the QCPI methodology and its dynamically enhanced versions, and the GQME kernel length. We find that the latter is always equal to the full Feynman-Vernon influence functional memory length, but considerably longer than the quantum memory length relevant to QCPI. We also compare the effort required to obtain converged long-time dynamics with these methods.

We follow the direct approach to generate the kernel from information contained in the RDM. [57, 64] This approach necessitates the numerical evaluation of RDM derivatives, which increases the computational effort and in some cases requires some care. Alternatively, the kernel may be obtained from information contained in system-bath correlation functions.[53, 55] This approach also requires a substantial amount of additional effort, as well as additional work to code the appropriate correlation function expressions, and has already been explored in the context of constructing the GQME kernel from Ehrenfest dynamics.[65]

In section II we review the two path integral based approaches (QuAPI and QCPI) we employ to either obtain the memory kernel for use in the GQME, or to independently propagate the RDM to long times, and their computational costs. In section III we summarize the GQME approach and discuss the numerical procedure we employ. Section IV specializes to the spin-boson model, for which we give the kernel elements and discuss computational details. Our results for four sets of parameters are presented in section V, along with a discussion of the convergence characteristics and required effort of the various methods. Our conclusions are discussed in section VI.

II. Real-time path integral methods

Our focus is on the dynamical properties of a quantum mechanical system, described by the coordinate s and conjugate momentum p_s, which is in contact with an environment composed of d degrees of freedom with phase space variables $\mathbf{q},\mathbf{p}$. The total Hamiltonian may be written as

$$\hat{H} = H_{\text{sys}}\left(\hat{s},\hat{p}_s\right) + H_{\text{env}}\left(\hat{q},\hat{p}\right) + V_{\text{int}}\left(\hat{s},\hat{q}\right) \tag{2.1}$$

where $H_{\rm sys}$ and $H_{\rm env}$ describe the system and environment, respectively, and $V_{\rm int}$ describes their interaction.

In many situations, the Hamiltonian of the environment is (or is assumed to be) quadratic, giving rise to the common system-bath Hamiltonian,

$$\hat{H} = H_{\rm sys}\left(\hat{s},\hat{p}_s\right) + \sum_{j=1}^{d}\frac{\hat{p}_j^2}{2m_j} + \frac{1}{2}m_j\omega_j^2\left(q_j - \frac{c_j\hat{s}}{m_j\omega_j^2}\right)^2 \tag{2.2}$$

where ω_j and c_j are the bath frequencies and system-bath coupling coefficients.

The dynamical properties of the system can be obtained from the RDM,

$$\tilde{\rho}\left(s'',s',t\right) \equiv \left\langle s''\middle|\hat{\tilde{\rho}}(t)\middle|s'\right\rangle = {\rm Tr}_{\rm env}\left\langle s''\middle|e^{-i\hat{H}t/\hbar}\hat{\rho}(0)e^{i\hat{H}t/\hbar}\middle|s'\right\rangle. \tag{2.3}$$

In the limit $d\to\infty$ the RDM of the system-bath Hamiltonian exhibits dissipative dynamics. The collective parameters of the harmonic bath are captured in the spectral density function,[66]

$$J(\omega) = \frac{\pi}{2}\sum_j \frac{c_j^2}{m_j\omega_j}\delta\left(\omega-\omega_j\right). \tag{2.4}$$

The dynamics of the RDM for the system-bath Hamiltonian can be obtained via the numerically exact QuAPI algorithm,[2-9] which is derived using the quasi-adiabatic splitting of the system-bath propagator[2] with a time step $\Delta t = t/N$. The QuAPI expression of the system-bath RDM has the form

$$\begin{aligned}\tilde{\rho}\left(s_N^{\pm};N\Delta t\right) = \int ds_0^{\pm}\cdots\int ds_{N-1}^{\pm}\left\langle s_N^{+}\middle|e^{-i\hat{H}_{\rm sys}\Delta t/\hbar}\middle|s_{N-1}^{+}\right\rangle\cdots\left\langle s_1^{+}\middle|e^{-i\hat{H}_{\rm sys}\Delta t/\hbar}\middle|s_0^{+}\right\rangle \\ \times\tilde{\rho}\left(s_0^{\pm};0\right)\left\langle s_0^{-}\middle|e^{i\hat{H}_{\rm sys}\Delta t/\hbar}\middle|s_1^{-}\right\rangle\cdots\left\langle s_{N-1}^{-}\middle|e^{i\hat{H}_{\rm sys}\Delta t/\hbar}\middle|s_N^{-}\right\rangle F\left(s_0^{\pm},s_1^{\pm},\ldots,s_N^{\pm};\Delta t\right)\end{aligned} \tag{2.5}$$

where F is the QuAPI-discretized Feynman-Vernon influence functional.[43] If the initial density operator is a product of system and equilibrium bath components, the influence functional is given by[6]

$$F\left(s_0^{\pm},s_1^{\pm},\ldots,s_N^{\pm};\Delta t\right) = \exp\left\{-\frac{1}{\hbar}\sum_{k=0}^{N}\Delta s_k\sum_{k'=0}^{k}{\rm Re}\,\eta_{kk'}\Delta s_{k'} + 2i\,{\rm Im}\,\eta_{kk'}\bar{s}_{k'}\right\} \tag{2.6}$$

where $\Delta s_k = s_k^{+} - s_k^{-}$ and $\bar{s}_k = \frac{1}{2}(s_k^{+}+s_k^{-})$ and the superscripts denote forward and backward path coordinates. A bath which initially is in equilibrium with a specific state of the system (e.g. the donor state in an electron transfer process) leads to a modified influence functional.[67] The $\eta_{kk'}$ coefficients introduce time-nonlocal interactions between the k and k' time points, which constitute the path integral manifestation of the bath-induced memory. These coefficients are available in terms of spectral density integrals,[6] and can also be obtained directly from the force autocorrelation function of the bath.[68]

In real-time path integral calculations the system coordinate is also discretized into n grid values using a system-specific discrete variable representation[69] (DVR). All integrals in Eq. (2.5) are then replaced by sums, and the influence functional is evaluated at the DVR eigenvalues.[70] For a given initial condition, there are n^N forward paths and an equal number of backward paths, such that evaluation of the discretized path integral expression requires summing n^{2N} terms.

The finite memory of dissipative environments allows a tensor decomposition of the path sum, which leads to the iterative i-QuAPI scheme.[4, 5] The basic i-QuAPI algorithm requires the storage of $n^{2L_{\mathrm{QuAPI}}}$ discrete system path segments, where L_{QuAPI} is the maximum value of $k-k'$ in Eq. (2.6); this parameter equals the number of time steps required to span the influence functional memory length. Each step in the i-QuAPI procedure involves $n^{2L_{\mathrm{QuAPI}}+2}$ operations. For propagation of the RDM to N path integral steps, the i-QuAPI methodology requires a total of $n^{2L_{\mathrm{QuAPI}}+2}N$ calculations.

However, a large fraction (and often the majority) of the $n^{2L_{\mathrm{QuAPI}}}$ paths make an exponentially small contribution and may be dropped. There are several ways of filtering out unimportant path segments.[7, 8, 10, 46] One very efficient such scheme is based on 'blips',[1] i.e. $\Delta s_k \neq 0$ terms. In fact, a restructuring of the forward-backward sum in Eq. (2.5) in terms of blips and sojourns (time points where the coordinates of forward and backward paths are identical) leads to an exponential reduction of the number of operations even without dropping any paths, and the contribution of path pairs with many blips is exponentially small in the incoherent regime, allowing elimination of multi-blip segments.[44] The blip-summed path integral (BSPI) reduces the number of integrand evaluations of the full path sum to $M \ll n^{2L_{\mathrm{QuAPI}}}$, allowing efficient evaluation of the path integral in cases of very long memory. A very efficient, iterative version of the BSPI algorithm is also available.[45]

In the case of anharmonic environments, the evolution of the RDM may be obtained using the QCPI formulation.[35-37] The QCPI expression is identical to Eq. (2.5), but the influence functional is now evaluated within a stationary phase approximation to the forward-backward bath propagator.[71-73] This procedure leads to an expression that involves classical trajectories and thus may be used with general, anharmonic environments. In the special case of a harmonic bath, stationary phase procedures are exact and reproduce the Feynman-Vernon influence functional.[35, 71, 72] After rearranging the path sum and the integral with respect to the phase space variables that specify trajectory initial conditions, the QCPI expression takes the form

$$\begin{aligned}\tilde{\rho}\left(s_N^{\pm};N\Delta t\right)=\int d\mathbf{q}_0\int d\mathbf{p}_0 P\left(\mathbf{q}_0,\mathbf{p}_0\right)\int ds_0^{\pm}\cdots\int ds_{N-1}^{\pm}\left\langle s_N^{+}\left|\hat{U}_{\mathrm{ref}}\left(N\Delta t,(N-1)\Delta t\right)\right|s_{N-1}^{+}\right\rangle\\ \cdots\left\langle s_1^{+}\left|\hat{U}_{\mathrm{ref}}\left(\Delta t,0\right)\right|s_0^{+}\right\rangle\tilde{\rho}\left(s_0^{\pm};0\right)\left\langle s_0^{-}\left|\hat{U}_{\mathrm{ref}}^{\dagger}\left(\Delta t,0\right)\right|s_1^{-}\right\rangle\\ \cdots\left\langle s_{N-1}^{-}\left|\hat{U}_{\mathrm{ref}}^{\dagger}\left(N\Delta t,(N-1)\Delta t\right)\right|s_N^{-}\right\rangle e^{\frac{i}{\hbar}\Delta\Phi\left(q_0,p_0;s_0^{\pm},s_1^{\pm},\ldots,s_N^{\pm}\right)}\end{aligned}\tag{2.7}$$

where $P(\mathbf{q}_0,\mathbf{p}_0)$ is the phase space distribution of the environment (i.e. either the classical Boltzmann factor or the quantized Wigner distribution[74]), $\hat{U}_{\mathrm{ref}}$ is the time evolution operator for a time-dependent system Hamiltonian augmented by the system-environment interaction along a chosen reference trajectory,[49] and $\Delta\Phi$ is the difference of action integrals along the forward and backward system paths. This phase contains all dynamical effects due to the interaction of the system with its environment. The numerical evaluation of the Wigner distribution involves a multidimensional Fourier-type integral, but several approximations as well as path integral-based methods are available for this task.[75-81]

A classical trajectory in the QCPI expression is integrated subject to the sequence of forces exerted by the system along each discrete path. This dependence leads to exponential proliferation of classical trajectories with the number of path integral time steps. This seemingly peculiar feature is the quantum-classical manifestation of influence functional memory.[35, 82] Just as in the case of the QuAPI expression, the memory quenching effects of the environment may be exploited to obtain at the i-QCPI decomposition, which maintains a constant number of trajectories.[36]

The incorporation of the action along reference trajectories in the system propagator[49] is equivalent to including the real part of the influence functional, that is, the reference propagators completely account for the "classical" memory.[47] Thus, the path-specific "back-reaction" $\Delta\Phi$ needs to capture only the "quantum" memory,[82] which is often considerably shorter than the classical memory. Further, the reference propagator is accurate over larger time steps. The combination of a shorter memory length and a larger time step enables convergence of the i-QCPI expression with L values that are considerably shorter than those in an i-QuAPI calculation.

Further, the reference trajectory is allowed to hop between the system states at each successive time step by a dynamically consistent state hopping (DCSH) scheme.[48] This procedure captures some of the quantum memory into the effective system propagators, rendering the i-QCPI memory length $L\Delta t$ even shorter.

III. Generalized quantum master equation

The Nakajima-Zwanzig[50, 51] GQME for propagation of the RDM is formally exact and is given by

$$i\hbar\frac{d}{dt}\hat{\tilde{\rho}}(t)=\hat{\mathcal{L}}_{\rm sys}\hat{\tilde{\rho}}(t)-i\hbar\int_0^t dt'\,\hat{\mathcal{K}}(t-t')\hat{\tilde{\rho}}(t')+i\hbar\hat{\mathcal{I}}(t)\,, \tag{3.1}$$

where the system Liouvillian superoperator is defined as $\mathcal{L}_{\rm sys}\cdot=\left[H_{sys},\cdot\right]$, $\mathcal{K}$ is the memory kernel which contains all the effects arising from the system-environment interaction, and the inhomogeneous term $\mathcal{I}$ vanishes for a separable initial condition $\rho(0)=\tilde{\rho}(0)\rho_{\rm env}(0)$. Since the kernel generally tends to be short-lived in comparison with the desired dynamics, Eq. (3.1) offers an avenue for obtaining the evolution of the RDM over time lengths much longer than the environment-induced memory. However, the memory kernel generally is not known. Here we explore the use of real-time path integral methods to generate the short-time kernel, for use in the GQME.

Since the system is described in terms of discrete states, we switch to matrix notation. We observe that

$$\begin{aligned}\tilde{\rho}_{jk}(t)&=\mathrm{Tr}_{\rm env}\left\langle j\left|e^{-i\hat{H}t/\hbar}\hat{\rho}(0)e^{i\hat{H}t/\hbar}\right|k\right\rangle\\&=\sum_{l,m}\mathrm{Tr}_{\rm env}\left\langle j\left|e^{-i\hat{H}t/\hbar}\right|l\right\rangle\left\langle l\left|\hat{\tilde{\rho}}(0)\right|m\right\rangle\hat{\rho}_{\rm env}(0)\left\langle m\left|e^{i\hat{H}t/\hbar}\right|k\right\rangle\\&=\sum_{l,m}\tilde{\mathcal{U}}_{jklm}(t)\tilde{\rho}_{lm}(0)\end{aligned} \tag{3.2}$$

where $\tilde{\boldsymbol{\mathcal{U}}}(t)$ is the $n^2\times n^2$ time evolution matrix for the RDM, with elements

$$\tilde{\mathcal{U}}_{jklm}(t)\equiv\mathrm{Tr}_{\rm env}\left\langle j\left|e^{-i\hat{H}t/\hbar}\right|l\right\rangle\hat{\rho}_{\rm env}(0)\left\langle m\left|e^{i\hat{H}t/\hbar}\right|k\right\rangle, \tag{3.3}$$

i.e., $\tilde{\mathcal{U}}_{jklm}(t)$ is the RDM element $\tilde{\rho}_{jk}(t)$ for the initial condition $\tilde{\rho}_{l'm'}(0)=\delta_{ll'}\delta_{mm'}$. The RDM evolution matrix may be used as input for obtaining the memory kernel according to the equation [57, 64]

$$i\hbar\,\mathcal{K}(t) = -i\hbar\,\ddot{\tilde{\mathcal{U}}}(t) + \dot{\tilde{\mathcal{U}}}(t)\cdot\mathcal{L}_{\rm sys} - i\hbar\int_0^t \dot{\tilde{\mathcal{U}}}(t-t')\cdot\mathcal{K}(t')\,dt' \,. \tag{3.4}$$

If the kernel memory is equal to $\tau_{\rm GQME}$, the lower limit in the time integral of Eq. (3.1) may be replaced by $t-\tau_{\rm GQME}$, and the GQME for the RDM becomes

$$i\hbar\frac{d}{dt}\tilde{\boldsymbol{\rho}}(t) = \mathcal{L}_{\rm sys}\cdot\tilde{\boldsymbol{\rho}}(t) - i\hbar\int_{t-\tau_{\rm GQME}}^{t} dt'\,\mathcal{K}(t-t')\cdot\tilde{\boldsymbol{\rho}}(t') \,. \tag{3.5}$$

Thus the RDM evolution operator $\tilde{\mathcal{U}}(t)$, along with its first and second derivatives, can be used to construct the GQME kernel over the memory time length, which can subsequently be used within the GQME to generate the long-time evolution of the RDM.

Earlier work[53] showed that the GQME kernel can be obtained in terms of self-consistent equations that involve time correlation functions of the system-bath coupling operator, and several other similar expressions are possible.[55] The approach given by Eq. (3.4) is simpler and convenient, as it requires only RDM elements, which are the target of all dynamics methods. However, Eq. (3.4) requires the numerical calculation of first and second derivatives, which requires a dense time grid and can be problematic if the RDM values contain statistical noise.

The RDM elements required to obtain the exact GQME kernel at the time points Δt, $2\Delta t$,…, $L_{\rm GQME}\Delta t$ using a path integral method (without path filtering and without utilizing symmetry properties) with time step Δt involve the following calculations: Generating the n^2 elements of the RDM at the time Δt requires n^2 terms from each initial condition; obtaining the RDM elements at the time $2\Delta t$ requires summing the amplitudes along n^4 paths; for the final time point $L_{\rm GQME}\Delta t$ one needs to sum $M = n^{2L_{\rm GQME}}$ path amplitudes. Thus, obtaining all elements of the RDM up to the GQME kernel memory length $\tau_{\rm GQME} = L_{\rm GQME}\Delta t$ for the n^2 possible initial conditions involves evaluating a total of $n^2\cdot(n^2+n^4+\cdots+n^{2L_{\rm GQME}}) = n^4(n^{2L_{\rm GQME}}-1)/(n^2-1)$ integrand terms.

The time derivatives are evaluated numerically. However, since the path integral time step Δt is chosen as large as possible, a much finer spacing of the data values is required to ensure smooth and stable first and second derivatives of the RDM evolution matrix. For this reason, path integral calculations must be run to generate $r \simeq 10$ data points per path integral time step. Thus, a total of $r\,n^4(n^{2L_{\rm GQME}}-1)/(n^2-1)$ integrand evaluations must be performed to obtain the GQME kernel matrix over the necessary memory length.

IV. Application to dissipative two-level systems and numerical procedures

We apply the QuAPI and QCPI methods to obtain the memory kernel and GQME dynamics for two-level systems coupled to harmonic dissipative baths. The system Hamiltonian is

$$\hat{H}_{\rm sys} = -\hbar\Omega\left(|R\rangle\langle L| + |L\rangle\langle R|\right) + \varepsilon\left(|R\rangle\langle R| - |L\rangle\langle L|\right) \tag{4.1}$$

where $|R\rangle, |L\rangle$ are the 'right' and 'left' TLS states. For notational clarity, we unfold the RDM developing from a specific initial condition to a 4-component vector. The system Liouvillian becomes

$$\mathcal{L}_{\text{sys}} = \begin{pmatrix} 0 & \hbar\Omega & -\hbar\Omega & 0 \\ \hbar\Omega & 2\varepsilon & 0 & -\hbar\Omega \\ -\hbar\Omega & 0 & -2\varepsilon & \hbar\Omega \\ 0 & -\hbar\Omega & \hbar\Omega & 0 \end{pmatrix} \tag{4.2}$$

The memory kernel for the dissipative TLS satisfies the symmetry relations[51] $\mathcal{K}_{\text{RLRR}} = \mathcal{K}^*_{\text{LRRR}}$, $\mathcal{K}_{\text{RLRL}} = \mathcal{K}^*_{\text{LRLR}}$, $\mathcal{K}_{\text{RLLR}} = \mathcal{K}^*_{\text{LRRL}}$ and $\mathcal{K}_{\text{RLLL}} = \mathcal{K}^*_{\text{LRLL}}$. Further, $\mathcal{K}_{\text{RR}ij} = \mathcal{K}_{\text{LL}ij} = 0$, thus there only four independent kernel elements: $\mathcal{K}_{\text{RLRR}}, \mathcal{K}_{\text{RLRL}}, \mathcal{K}_{\text{RLLR}}, \mathcal{K}_{\text{RLLL}}$.

The TLS RDM propagator $\tilde{\mathcal{U}}$ is given by the 4×4 matrix,

$$\tilde{\mathcal{U}}(t) = \begin{pmatrix} \tilde{\rho}^{\text{RR}}_{\text{RR}}(t) & \tilde{\rho}^{\text{RL}}_{\text{RR}}(t) & \tilde{\rho}^{\text{LR}}_{\text{RR}}(t) & \tilde{\rho}^{\text{LL}}_{\text{RR}}(t) \\ \tilde{\rho}^{\text{RR}}_{\text{RL}}(t) & \tilde{\rho}^{\text{RL}}_{\text{RL}}(t) & \tilde{\rho}^{\text{LR}}_{\text{RL}}(t) & \tilde{\rho}^{\text{LL}}_{\text{RL}}(t) \\ \tilde{\rho}^{\text{RR}}_{\text{LR}}(t) & \tilde{\rho}^{\text{RL}}_{\text{LR}}(t) & \tilde{\rho}^{\text{LR}}_{\text{LR}}(t) & \tilde{\rho}^{\text{LL}}_{\text{LR}}(t) \\ \tilde{\rho}^{\text{RR}}_{\text{LL}}(t) & \tilde{\rho}^{\text{RL}}_{\text{LL}}(t) & \tilde{\rho}^{\text{LR}}_{\text{LL}}(t) & \tilde{\rho}^{\text{LL}}_{\text{LL}}(t) \end{pmatrix} \tag{4.3}$$

where the subscripts on the RDM elements correspond to the states at the final time, while the superscripts label the initial conditions, i.e.,

$$\tilde{\rho}^{ij}_{ab}(t) = \text{Tr}_{\text{env}}\left(\langle a|\hat{U}(t)|i\rangle\langle i|\hat{\rho}(0)|j\rangle\langle j|\hat{U}^{\dagger}(t)|b\rangle\right). \tag{4.4}$$

In order to compare results obtained with QuAPI and QCPI, we employ harmonic baths described in terms of spectral densities that have the common Ohmic form,[66]

$$J(\omega) = \tfrac{1}{2}\pi\hbar\xi\omega e^{-\omega/\omega_c} \tag{4.5}$$

where the dimensionless Kondo parameter ξ quantifies the TLS-bath coupling strength and ω_c is the cutoff frequency. We evaluate the kernel for the four possible initial conditions by performing non-iterative QuAPI or QCPI calculations. Each of these involves summing the path integral amplitudes over the GQME memory length, and (in the case of QCPI) integrating classical trajectories with initial conditions sampled by a Monte Carlo process. Implementation of the QCPI methodology requires discretization of the bath in terms of d frequencies and coupling constants. We have followed the logarithmic discretization[83] with $d = 60$. The QCPI results presented in the next section were performed with solvent-driven reference propagators,[49] utilizing the DCSH branching scheme,[48] and employed a total of 60,000 initial conditions sampled by Monte Carlo[84] from the thermal Wigner distribution of the harmonic bath (which is available analytically). We have found that using $r \simeq 10$ RDM values within each path integral time step generates a sufficient number of data points for derivative evaluation. Thus the total number of amplitudes over the GQME memory length is $160(4^{L_{\text{GQME}}} - 1)/3$.

In the case of QuAPI, one could alternatively interpolate the RMD results to obtain r points in each Δt interval, avoiding additional QuAPI runs. We have found interpolation procedures can introduce some error, in particular in cases where the RDM exhibits oscillatory behavior, which is undesirable when using an exact method. Since such error would depend on the choice of interpolation function (as well as the spacing of the input RDM data), checking the accuracy of the results would require additional effort.

Once the path integral results for all initial conditions have been obtained, we further fit them to cubic splines, to generate time points on a still finer time grid, with a time spacing of $0.0005\Omega^{-1}$, for derivative evaluation. In the case of QCPI, smoothing the RDM results is necessary because of the unavoidable Monte Carlo error. Generally, we find that obtaining QCPI RDM derivatives requires some care: different choices of the smoothing algorithm affect the accuracy of the kernel, and can even alter the GQME results in some regimes. Finally, we integrate the GQME using a first order forward finite difference procedure to obtain the RDM elements for longer times. To this end, we approximate the derivative of $\tilde{\rho}$ as its first order forward finite difference. Our integration procedure is different from the self-consistent scheme employed in Ref. [64].

For each of the calculations, numerically exact results were obtained using the i-QuAPI (or its blip decomposition, i-BSPI) and the i-QCPI methods. We present the population dynamics and report the time step and memory length required for convergence of each method (to within 0.01 in the monitored state population). We also compare these results to those obtained by integrating the GQME with a memory kernel obtained using QuAPI and, when possible, QCPI.

V. Results

(a) Model 1: Symmetric TLS with moderate dissipation at low temperature

The first model involves a symmetric TLS linearly coupled to a harmonic bath with $\omega_c = 5\Omega$, $\xi = 0.3$ at a low temperature corresponding to $\hbar\Omega\beta = 5$. The bath is initially in Boltzmann equilibrium, isolated from the TLS. With these parameters the population of the initial state exhibits strongly damped oscillations.[35] Numerically exact results were obtained using the i-QuAPI method (without path filtering) with a time step of $\Omega\Delta t = 0.2$ and $L_{\mathrm{QuAPI}} = 6$, thus the QuAPI memory (i.e. the span of the Feynman-Vernon influence functional nonlocality) is $\Omega\tau_{\mathrm{QuAPI}} = 1.2$. Our i-QCPI calculations with $\Omega\Delta t = 0.25$ and $L_{\mathrm{QCPI}} = 3$ reproduced (within 0.01) the converged i-QuAPI results, so the QCPI memory length is $\Omega\tau_{\mathrm{QCPI}} = 0.75$. The reason for the much shorter memory requirements of i-QCPI is the incorporation of bath dynamics into effective system propagators, which automatically capture at the very least all classical memory (the real part of the exponent of the influence functional), and (through DCSH branching) even a portion of the quantum nonlocality, leaving just the remaining quantum memory to be accounted for via the path integral. The use of reference propagators also allows a larger time step in QCPI. In fact, QCPI calculations with $\Omega\Delta t_{\mathrm{QCPI}} = 0.3$ produced indistinguishable results. Through a combination of shorter memory and larger time step, the i-QCPI calculations converged with a much smaller value of L compared to that required in i-QuAPI, which employs the full Feynman-Vernon influence functional.

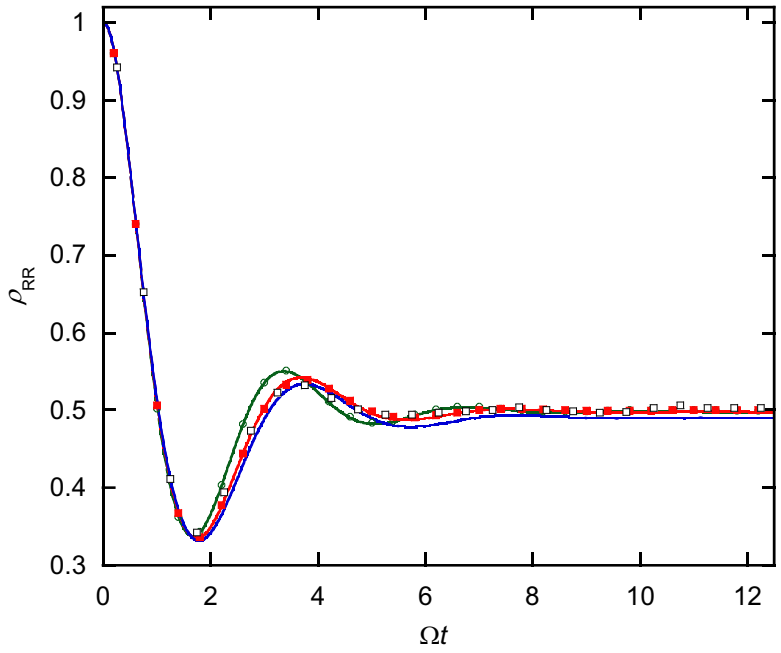

Fig 1. Population dynamics of model 1. Green hollow circles: unconverged i-QuAPI results with $\tau = 0.4$. Green line: unconverged QuAPI-GQME results with $\tau = 0.4$. Red filled squares: converged i-QuAPI results with $\Omega\tau_{\mathrm{QuAPI}} = 1.2$, $L_{\mathrm{QuAPI}} = 6$. Red line: converged QuAPI-GQME results with $\Omega\tau_{\mathrm{GQME}} = 1.2$. Black hollow squares: i-QCPI results with $\Omega\tau_{\mathrm{QCPI}} = 0.75$, $L_{\mathrm{QCPI}} = 3$. Blue line: QCPI-GQME results with $\Omega\tau_{\mathrm{GQME}} = 1.2$.

Figure 1 shows the converged population dynamics of an initially right-localized state, along with shorter memory results. The memory length required to converge the GQME calculation with the QuAPI kernel, $\Omega\tau_{\mathrm{GQME}} = 1.2$, is exactly the same as the memory required in the i-QuAPI calculation for the same accuracy. Further, we find that the results obtained from the GQME using the exact kernel with *any* chosen memory length are identical to those of the i-QuAPI calculation with the same memory length. Also shown in Fig. 1 are GQME results with a memory kernel generated from the QCPI calculations with $\Omega\tau_{\mathrm{GQME}} = 1.2$. While these results are converged with respect to the GQME memory, small deviations from the exact i-QCPI and i-QuAPI results are seen. These arise from numerical error in the smoothing procedure and derivative evaluation.

Figure 2 shows the independent elements of the GQME kernel obtained from our QuAPI calculations. Some numerical noise is observed, which arises (even in the absence of Monte Carlo error) from the numerical derivative evaluations and is most pronounced in the imaginary part. Still, the imaginary part is rather small, and this noise does not prevent the integration of the GQME. It is seen that the kernel elements decay to almost zero within the memory time interval. Extending the memory time in order for the kernel to attain values closer to zero does not lead to a noticeable change of the population dynamics.

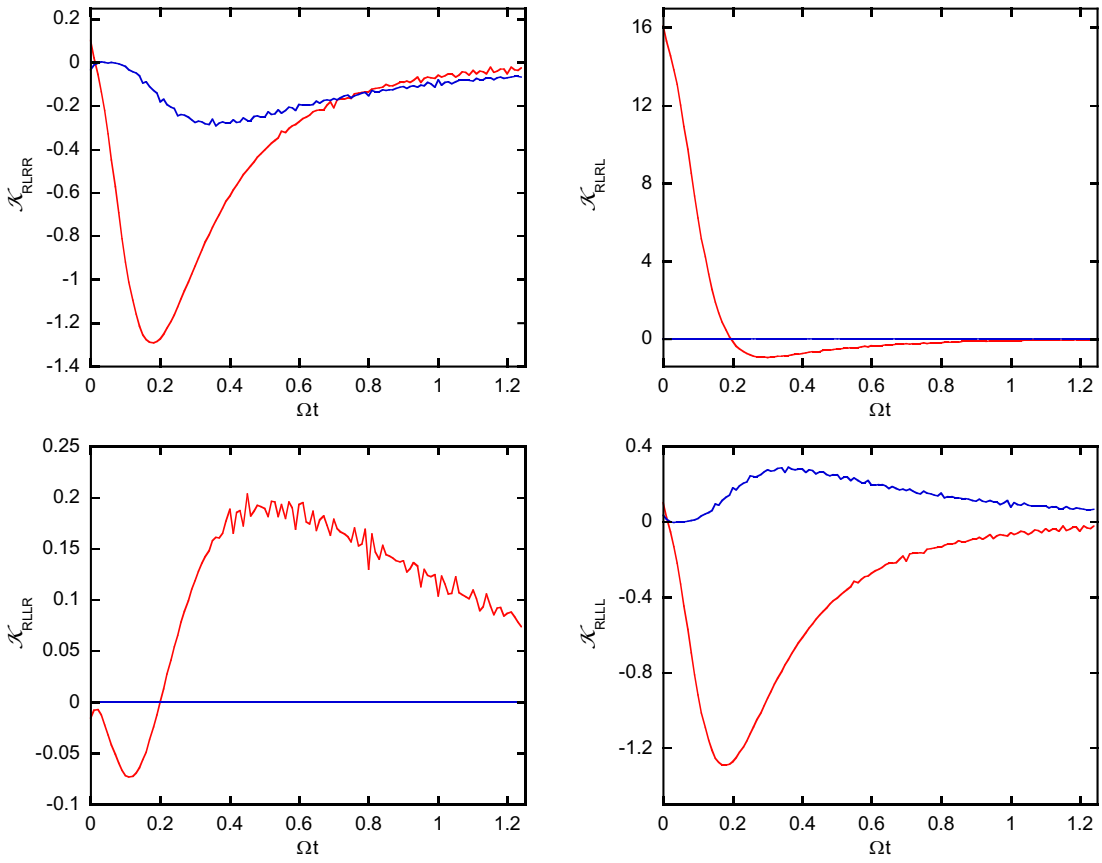

Fig. 2. Real (red) and imaginary (blue) parts of the kernel elements for model 1.

(b) Model 2: Symmetric TLS with strong dissipation at high temperature

The second model employs a symmetric TLS coupled to a strongly dissipative bath with $\omega_c = 2.5\Omega$ and $\xi = 1.2$ at a high temperature corresponding to $\hbar\Omega\beta = 0.2$. In this regime, the coherent oscillations of the bare system are completely quenched and the populations show monotonic relaxation.[35] The TLS is initially in the R state, while the bath is in thermal equilibrium, isolated from the system.

Figure 3 shows the population of the R state as obtained through i-QuAPI calculations with $\Omega\Delta t_{\mathrm{QuAPI}} = 0.15$ and also from the GQME with the QuAPI kernel. Again, unconverged i-QuAPI and QuAPI-GQME results with $\Omega\tau = 0.3$ are practically indistinguishable, and the GQME kernel memory $\Omega\tau_{\mathrm{GQME}} = 1.2$ is equal to the converged i-QuAPI memory (i.e. the influence functional nonlocality), $\Omega\tau_{\mathrm{QuAPI}} = 1.2$, which spans $L_{\mathrm{QuAPI}} = 8$ path integral time steps.

For this model, in which the population follows a simple, monotonic decay, we found it easier to obtain stable GQME results with a kernel computed via QCPI calculations. While the i-QuAPI and QuAPI-GQME formulations require the same memory to converge, i-QCPI calculations are again seen to converge considerably faster. This trend is illustrated in Figure 4, which shows the memory requirements of i-QCPI in comparison to the GQME. It is seen that the i-QCPI results with memory length equal to $\Omega\tau_{\mathrm{QCPI}} = 0.3$ are in quantitative agreement with the converged i-QuAPI results. Again, the reason for the much shorter memory requirements of i-QCPI is the need to account for only some of the quantum memory. The

reduction of required memory length in the i-QCPI calculation is even more pronounced in the case of model 2, because the quantum memory is less significant in the incoherent regime. The QCPI-GQME results with the same memory length are rather poor, as a fourfold increase in memory is required to converge the GQME. Further, the inclusion of much of the bath dynamics into reference QCPI propagators allows again a twofold increase of the path integral time step, and results obtained with $\Omega\Delta t_{\mathrm{QCPI}} = 0.3$ are indistinguishable. The i-QCPI results obtained with $L_{\mathrm{QCPI}} = 1$ are indistinguishable from the converged i-QuAPI results. Thus, the use of QCPI leads to a dramatic gain in convergence in this regime compared to i-QuAPI. However, the QCPI advantage is lost when the method is combined with the GQME, as the GQME kernel spans the full influence functional memory.

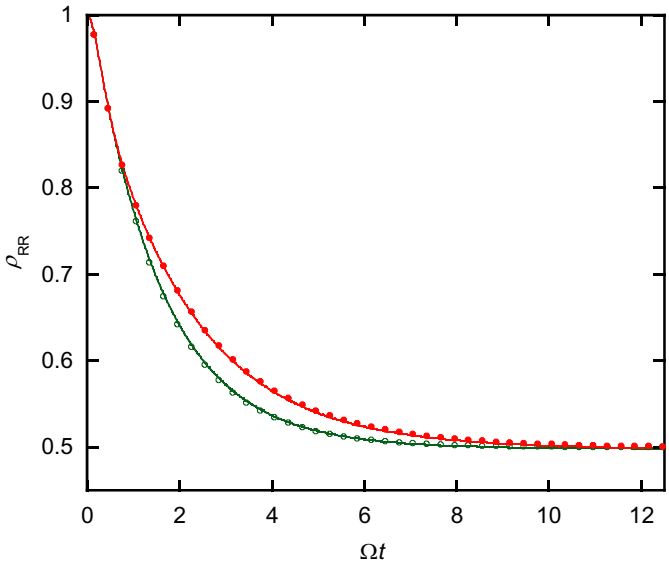

Fig 3. Population dynamics of model 2. Green hollow circles: unconverged i-QuAPI results with $\Omega\tau = 0.3$. Green line: unconverged QuAPI-GQME results with $\Omega\tau = 0.3$. Red filled circles: converged i-QuAPI results with $\Omega\Delta t_{\mathrm{QuAPI}} = 0.15$, $L_{\mathrm{QuAPI}} = 8$, $\Omega\tau_{\mathrm{QuAPI}} = 1.2$. Red line: converged QuAPI-GQME results with $\Omega\tau_{\mathrm{GQME}} = 1.2$.

The independent elements of the memory kernel obtained from the QuAPI calculations are presented in Figure 5.

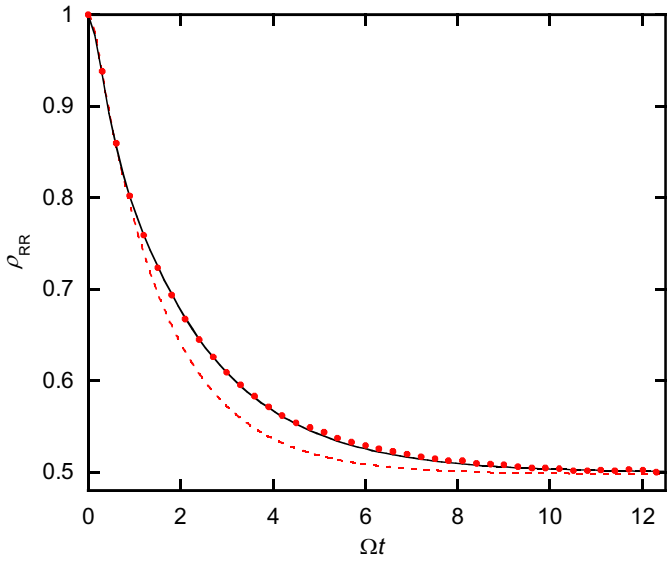

Fig 4. Population dynamics of model 2. Black line: converged i-QuAPI results. The full memory is $\Omega\tau_{\mathrm{QuAPI}} = \Omega\tau_{\mathrm{GQME}} = 1.2$. Red filled circles: converged i-QCPI results with $\Omega\tau_{\mathrm{QCPI}} = 0.3$, $L_{\mathrm{QCPI}} = 1$. Red dashed line: unconverged QCPI-GQME results with $\Omega\tau = 0.3$.

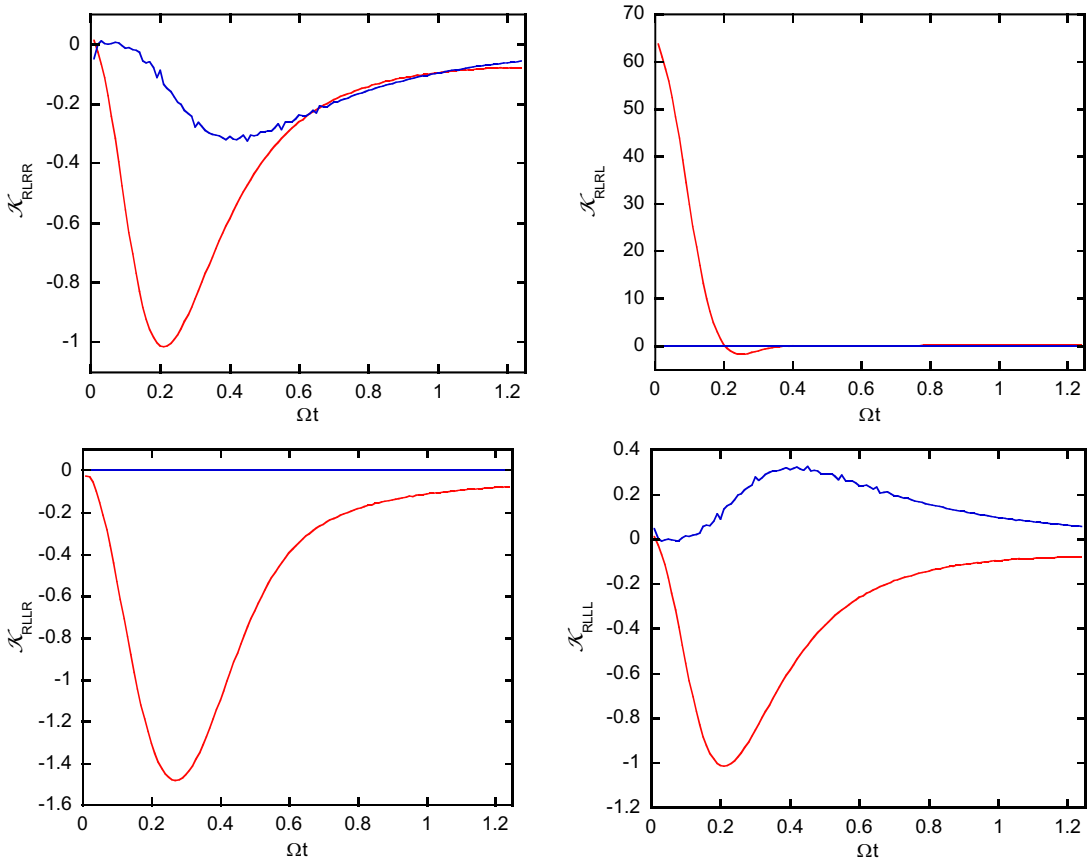

Fig. 5. The independent elements of the kernel for model 2. Red lines: real part. Blue lines: imaginary part.

(c) Model 3: Asymmetric TLS weakly coupled to high-frequency bath at low temperature

The third model is an asymmetric TLS with $\varepsilon = \hbar\Omega$, weakly coupled to a fast bath with $\omega_c = 7.5\Omega$ and $\xi = 0.1$. This regime shows pronounced quantum mechanical behavior characterized by persistent oscillations in the populations.[36] The bath is initially in thermal equilibrium at a very low temperature of $\hbar\Omega\beta = 5$. Since $\hbar\omega_c\beta = 37.5$, this bath is highly quantum mechanical.

Figure 6 shows population dynamics for an initially right-localized state obtained by i-QuAPI, as well as using the GQME with QuAPI kernels. The converged i-QuAPI results with $\Omega\Delta t_{\mathrm{QuAPI}} = 0.2$ and $L_{\mathrm{QuAPI}} = 10$, i.e., $\Omega\tau_{\mathrm{QuAPI}} = 2$, are identical with the QuAPI-GQME results obtained with the same memory length, $\Omega\tau_{\mathrm{GQME}} = 2$. Also, unconverged i-QuAPI and QuAPI-GQME results using a much shorter memory length $\Omega\tau = 0.4$ are indistinguishable, confirming once again that memory dependence of the GQME is exactly the same as in the i-QuAPI algorithm. Also shown are results obtained through i-QCPI calculations, which converge with the time step $\Omega\Delta t_{\mathrm{QCPI}} = 0.25$ and a shorter memory, $\Omega\tau_{\mathrm{QCPI}} = 1.25$. The QCPI reduction of memory length is less dramatic in this case compared to that observed in model 2, because the highly quantum mechanical nature of the bath implies that the quantum mechanism of decoherence is quite significant. Yet, through the increased time step and shorter memory, the QCPI calculations converged with $L_{\mathrm{QCPI}} = 5$, reducing the number of forward-backward paths required to span the memory length from $4^{10} \simeq 10^6$ in i-QuAPI to $4^5 \simeq 10^3$. In this case we were unable to obtain stable and accurate GQME kernels from QCPI calculations, because the oscillatory nature of the populations complicated the smoothing procedure. However, we note again that QCPI calculations to generate the GQME kernel would require the $L = 8$ to span the full GQME memory. Representative kernel elements for this model are given in Figure 7.

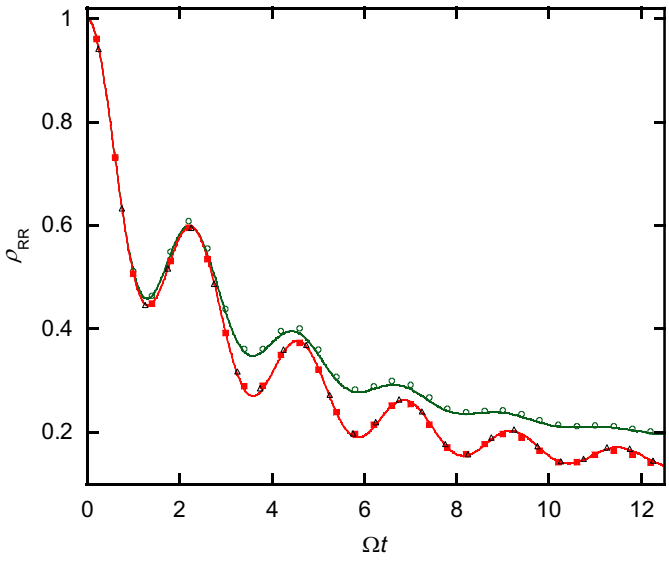

Fig 6. Population dynamics of model 3. Green hollow circles: unconverged i-QuAPI results with $\Omega\tau = 0.4$. Green line: unconverged QuAPI-GQME results with $\Omega\tau = 0.4$. Red filled squares: converged i-QuAPI results with $\Omega\Delta t_{\mathrm{QuAPI}} = 0.2$, $L_{\mathrm{QuAPI}} = 10$, $\Omega\tau_{\mathrm{QuAPI}} = 2$. Red line: converged QuAPI-GQME results with $\Omega\tau_{\mathrm{gQME}} = 2$. Black hollow triangles: i-QCPI results with $\Omega\tau_{\mathrm{QCPI}} = 1.25$, $L_{\mathrm{QCPI}} = 5$.

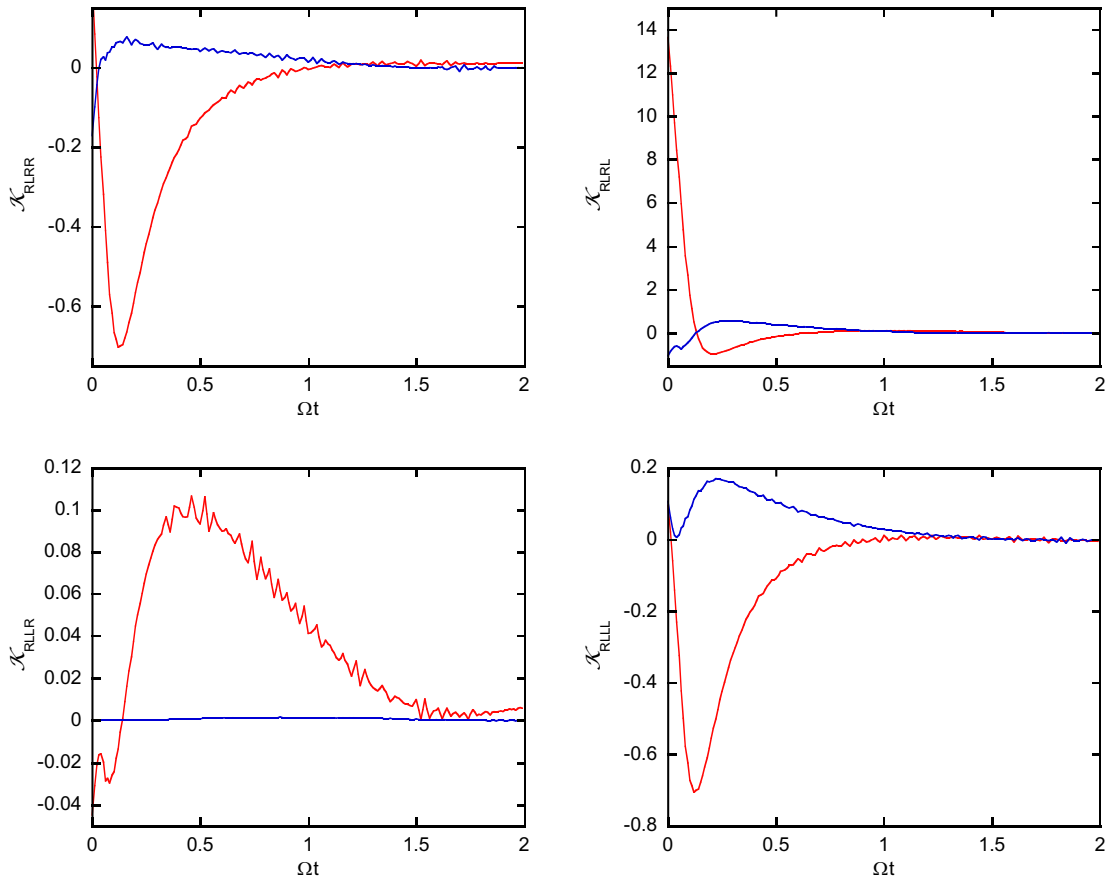

Fig. 7. The elements of the memory kernel for model 3. Red line: real part. Blue line: imaginary part.

(d) Model 4: Symmetric TLS strongly coupled to slow bath at an intermediate temperature

The last model uses a symmetric TLS coupled to a strongly dissipative, sluggish bath with $\omega_c = \Omega$ and $\xi = 2$ at an intermediate temperature corresponding to $\hbar\Omega\beta = 1$.[48] The TLS is initially in the R state, while the bath is equilibrated with respect to the initial TLS state. These parameters correspond to a challenging regime, and calculations require small time steps as well as a long memory.

Figure 8 displays the time evolution of the population. Converged i-QCPI results are shown with $\Omega\Delta t_{\mathrm{QCPI}} = 0.25$ and $L_{\mathrm{QCPI}} = 8$, i.e. the QCPI memory length is $\Omega\tau_{\mathrm{QCPI}} = 2$. QuAPI calculations converged with a similar time step, $\Omega\Delta t_{\mathrm{QuAPI}} = 0.125$; however, the full memory exceeds the time length displayed in Fig. 8, $\Omega\tau_{\mathrm{QuAPI}} > 3$, thus raw i-QUAPI calculations are comfortably feasible for about half of the time shown. The blip decomposition extends the feasibility of path integral calculations with the full Feynman-Vernon influence functional to much longer times, reproducing the QCPI results. It is again seen that the unconverged GQME results are identical to the i-QuAPI results with the same memory length. Also shown in Fig. 8 are GQME results with the kernel generated from QCPI calculations with $\Omega\tau_{\mathrm{QCPI}} = 2$. The small deviations from the exact results even before the memory time is exceeded are the results of the smoothing procedures to compute derivatives.

The independent elements of the memory kernel obtained by QuAPI are presented in Figure 9.

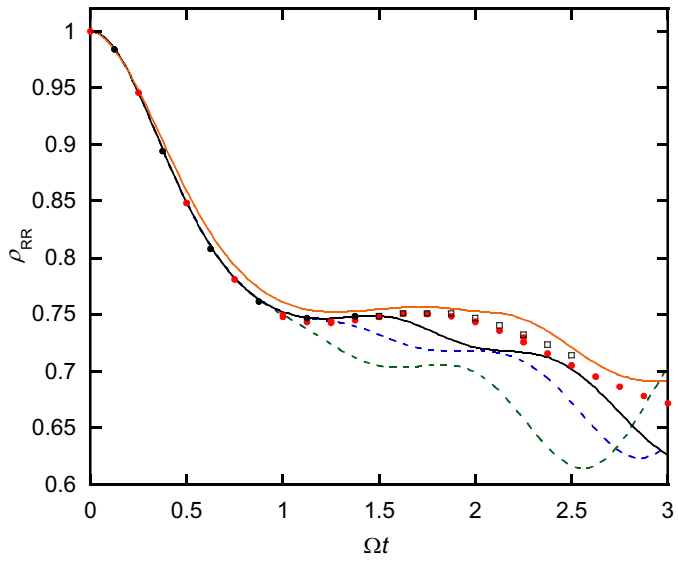

Fig. 8. Population dynamics of model 4. Red filled markers: converged i-QCPI results with $\Omega\Delta t_{\mathrm{QCPI}} = 0.25$, $L_{\mathrm{QCPI}} = 8$ ($\Omega\tau_{\mathrm{QCPI}} = 2$). Black circles: full QuAPI results (no memory truncation) with $\Omega\Delta t_{\mathrm{QuAPI}} = 0.125$. Hollow squares: full BSPI results (no memory truncation) with three blips and $\Omega\Delta t = 0.125$. Dashed green and blue lines and solid black line: unconverged GQME results with QuAPI kernels, $L = 6, 8$ and 11. Orange line: QCPI-GQME results with $L_{\mathrm{QCPI}} = 8$ ($\Omega\tau_{\mathrm{GQME}} = 2$).

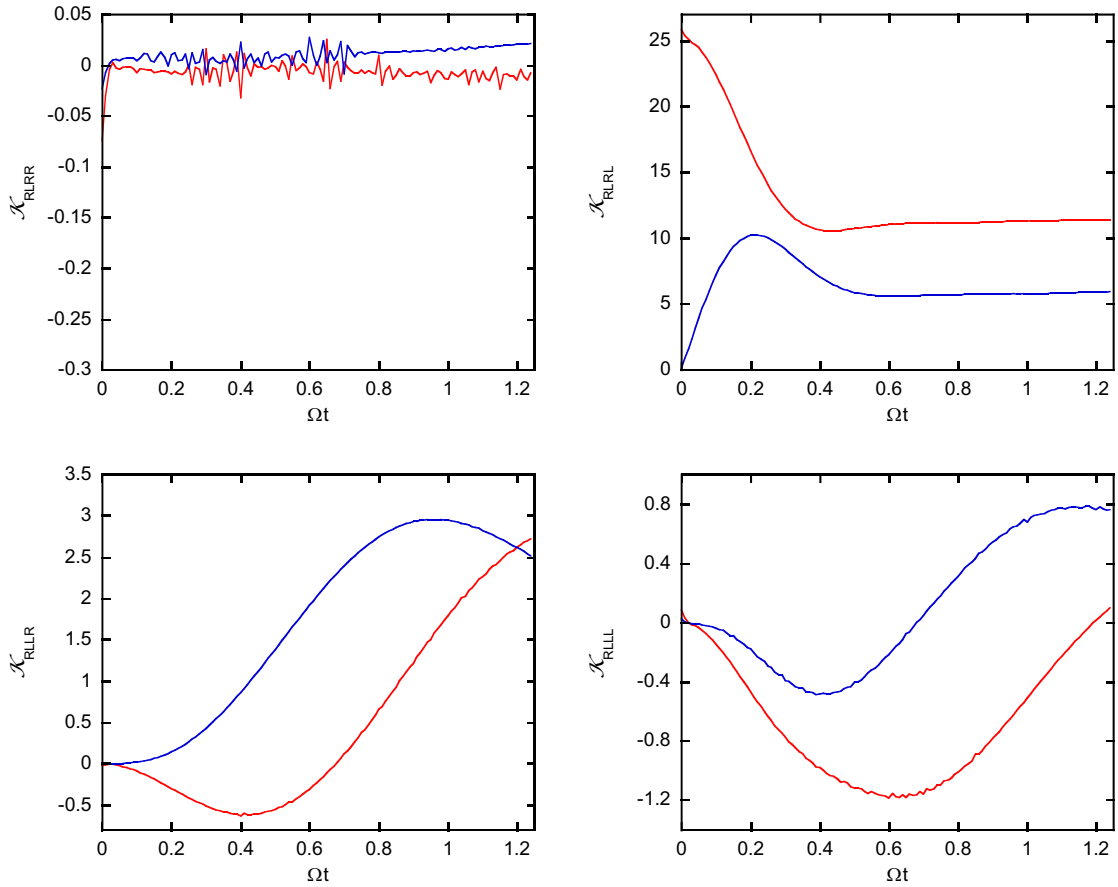

Fig. 9. Memory kernel elements for model 4. Red line: real part. Blue line: imaginary part.

The findings of our calculations on models 1-4, i.e. the memory times and numbers of path integral time steps required to span the memory time in each case, are summarized in Table 1. In all cases, we found that the GQME solution based on a numerically exact memory kernel reproduces the converged iterative path integral results with the same memory length. Further, we found that when the kernel memory is prematurely truncated, the unconverged GQME results agree exactly with the unconverged i-QuAPI results. This observation is another manifestation of the exact manner in which both formulations handle the dissipative effects of a bath on a quantum system. It is also in line with one's expectation of the properties of the GQME solution with a numerically exact kernel.[56]

We also found that the memory required to converge i-QCPI calculations is always shorter than the GQME kernel memory. This is a consequence of the ability of the QCPI methodology to incorporate the classical memory in its entirety, and also some of the remaining quantum memory, into effective system propagators that satisfy the closure property and need no path integral slicing. Because the classical memory is the dominant component of the influence functional nonlocality, its removal from the explicit path integral operations implies dramatic savings. However, these savings cannot be transferred to the GQME solution with a QCPI kernel. To use the GQME, one would need to run QCPI calculations with path segments longer than necessary in order to obtain the GQME kernel over its full memory length. The direct application of the i-QCPI algorithm is thus much more efficient. The i-QCPI propagator for each trajectory initial condition (the "quantum influence function") is also norm conserving[36] and thus stable over long propagation lengths.

Table 1. Summary of results for models 1-4.

	Parameters	$\Omega\tau_{\mathrm{GQME}} = \Omega\tau_{\mathrm{QuAPI}}$	$L_{\mathrm{GQME}} = L_{\mathrm{QuAPI}}$	$\Omega\tau_{\mathrm{QCPI}}$	L_{QCPI}
Model 1	$\varepsilon = 0, \hbar\Omega\beta = 5, \omega_c = 5\Omega, \xi = 0.3$	1.2	6	0.75	3
Model 2	$\varepsilon = 0, \hbar\Omega\beta = 0.2, \omega_c = 2.5\Omega, \xi = 1.2$	1.2	8	0.3	1
Model 3	$\varepsilon = \hbar\Omega, \hbar\Omega\beta = 5, \omega_c = 7.5\Omega, \xi = 0.1$	2	10	1.25	5
Model 4	$\varepsilon = 0, \hbar\Omega\beta = 1, \omega_c = \Omega, \xi = 2$	>3	>24	2	8

VI. Discussion and concluding remarks

The numerical calculations presented in section V indicate that in the case of system-bath Hamiltonians, the memory length of the GQME kernel is the same as the full memory required to converge i-QuAPI calculations with the same parameters. Setting $L_{\mathrm{GQME}} = L_{\mathrm{QuAPI}} \equiv L$, the number of integrand evaluations required to generate the GQME memory kernel from full path integral calculations is $r n^4 (n^{2L} - 1)/(n^2 - 1) \simeq 10 n^{2L+2}$. The procedure of interpolating, evaluating derivatives and integrating the GQME adds to the computation time, although these operations are not very demanding. Overall, the cost of the GQME approach seems comparable to that of an i-QuAPI calculation, which requires $N n^{2L+2}$ operations for propagation to N time steps. For very large values of N, the i-QuAPI calculation could become more expensive. However, the i-QuAPI scheme is norm-conserving and thus stable, while the stability and accuracy of the GQME solution over very long times would need to be tested. We also note that path filtering and the BSPI decomposition can dramatically reduce the computational effort required to generate the GQME kernel or to perform an iterative path integral calculation.

In addition to the computational cost described above and the overhead of processing the RDM data to obtain the GQME memory kernel, we note that the GQME approach requires substantial care to guarantee derivative stability and accuracy. The i-QuAPI matrix-vector procedure is simpler in this regard. Thus, the main appeal of the GQME approach is for situations of very long memory that does not permit storage of the array of path configurations that are needed in iterative path integral calculations. With the BSPI decomposition, storage of path segments is replaced by storage of blip configurations, [44, 45] which reduces the RAM demands of path integral methods by many orders of magnitude. Thus, the storage advantage of the GQME approach with a kernel computed by exact path integral methods may be more important for handling multi-state systems. Last, the use of GQME methods with time-dependent Hamiltonians, while possible in principle,[85] would require a new kernel calculation at every time step. System-dependent driving terms present no difficulty to iterative path integral methods. Since construction of the memory kernel is a tedious and time consuming process, the direct use of iterative path integral methods for propagation is much preferable in such cases.

Next, we focus on the more significant potential appeal of the GQME approach, in the context of simulating the dynamics of systems interacting with complex, anharmonic environments. In this paper we examined the possibility of employing the rigorous QCPI formulation to generate the GQME memory kernel. The findings of our calculations were summarized in Table 1. We found that the memory length required for convergence of the i-QCPI methodology is always shorter than the GQME kernel length. This fact stems from the two distinct contributions to the bath-induced memory, and the ability of the QCPI formulation to capture the entire classical component of this memory (which is associated with decoherence through absorption and stimulated emission of phonons),[47] as well as a portion of the remaining quantum memory (which arises from spontaneous phonon emission) within effective propagators.[37] This very attractive feature is lost once the QCPI kernel is inserted in the GQME, since the latter needs to be solved with the full memory. An all-path i-QCPI calculation to the time $N\Delta t$ (without filtering) requires the manipulation of $N n^{2L_{\mathrm{QCPI}}+2}$ terms from each trajectory initial condition, while a QCPI calculation of the GQME kernel would require the evaluation of $\sim 10 n^{2L_{\mathrm{GQME}}+2}$ terms (from each initial condition) with $L_{\mathrm{QCPI}} < L_{\mathrm{GQME}}$. The direct, iterative i-QCPI evaluation is thus much more efficient than the solution of the GQME with a QCPI-generated kernel. In addition, the direct i-QCPI calculation avoids the need for RDM smoothing that is required for derivative evaluation and which can be delicate because of unavoidable Monte Carlo error in the data.

Last, we note an additional advantage of the full i-QCPI approach. QCPI calculations employ full classical trajectories of the system's environment, which capture the true dynamical features of the medium that may include motions evolving over very long times. For example, protein conformational changes occur on the time scale of nanoseconds or even microseconds. Such structural changes, which can play a critical role in long-range biological electron transfer or isomerization reactions,[86-88] are fully accounted for in i-QCPI calculations. In order to capture the effects of such conformational rearrangements through a memory kernel, this kernel would need to span practically the entire time length of the process. More importantly, a calculation based on a pre-constructed memory kernel might seem to converge over a relatively short memory time, entirely missing important dynamical effects on the quantum process of interest by failing to account for the effects of a structurally different environment that develops much later. The advantage of full trajectory-based methods is very significant in this regard.

Acknowledgments

This material is based upon work supported by the National Science Foundation under Award CHE-1665281. We thank Eitan Geva for useful discussions.

References

1. Leggett, A. J.; Chakravarty, S.; Dorsey, A. T.; Fisher, M. P. A.; Garg, A.; Zwerger, M., Dynamics of the dissipative two-state system. *Rev. Mod. Phys.* **1987**, 59, 1-85.
2. Makri, N., Improved Feynman propagators on a grid and non-adiabatic corrections within the path integral framework. *Chem. Phys. Lett.* **1992**, 193, 435-444.
3. Makarov, D. E.; Makri, N., Path integrals for dissipative systems by tensor multiplication: condensed phase quantum dynamics for arbitrarily long time. *Chem. Phys. Lett.* **1994**, 221, 482-491.
4. Makri, N.; Makarov, D. E., Tensor multiplication for iterative quantum time evolution of reduced density matrices. I. Theory. *J. Chem. Phys.* **1995**, 102, 4600-4610.
5. Makri, N.; Makarov, D. E., Tensor multiplication for iterative quantum time evolution of reduced density matrices. II. Numerical methodology. *J. Chem. Phys.* **1995**, 102, 4611-4618.
6. Makri, N., Numerical path integral techniques for long-time quantum dynamics of dissipative systems. *J. Math. Phys.* **1995**, 36, 2430-2456.
7. Sim, E.; Makri, N., Tensor propagator with weight-selected paths for quantum dissipative dynamics with long-memory kernels. *Chem. Phys. Lett.* **1996**, 249, 224-230.
8. Sim, E.; Makri, N., Filtered propagator functional for iterative dynamics of quantum dissipative systems. *Comp. Phys. Commun.* **1997**, 99, 335-354.
9. Makri, N., Quantum dissipative systems: a numerically exact methodology. *J. Phys. Chem.* **1998**, 102, 4414-4427.
10. Sim, E., Quantum dynamics for a system coupled to slow baths: on-the-fly filtered propagator method. *J. Chem. Phys.* **2001**, 115, 4450-4456.
11. Shao, J.; Makri, N., Iterative path integral calculation of quantum correlation functions for dissipative systems. *Chem. Phys.* **2001**, 268, 1-10.
12. Shao, J.; Makri, N., Iterative path integral formulation of equilibrium correlation functions for quantum dissipative systems. *J. Chem. Phys.* **2002**, 116, 507-514.
13. Weiss, S.; Eckel, J.; Thorwart, M.; Egger, R., Iterative real-time path integral approach to nonequilibrium quantum transport. *Phys. Rev. B* **2008**, 77, 195316.
14. Segal, D.; Millis, A. J.; Reichman, D. R., Numerically exact path integral simulation of nonequilibrium quantum transport and dissipation. *Phys. Rev. B* **2010**, 82, 205323.
15. Simine, L.; Segal, D., Path integral simulations with fermionic and bosonic reservoirs: Transport and dissipation in molecular electronic junctions. *J. Chem. Phys.* **2013**, 138, 214111.
16. Makri, N., Path integral renormalization for quantum dissipative dynamics with multiple timescales. *Mol. Phys.* **2012**, 110, 1001-1007.
17. Richter, M.; Fingerhut, B. P., Coarse-grained representation of the quasiadiabatic propagator path integral for the treatment of non-Markovian long-time bath memory. *J. Chem. Phys.* **2017**, 146, 214101.
18. Nalbach, P.; Palm, P., Quasi-adiabatic path integral approach for quantum systems under the influence of multiple non-commuting fluctuations. *J. Chem. Phys.* **2018**, 149, 214103.
19. Straatsma, T. P.; Lovett, B. W.; Kirton, P., Efficient real-time path integrals for non-Markovian spin-bosonmodels. *New Journal of Physics* **2017**, 19, 093009.
20. Strathearn, A.; Kirton, P.; Kilda, D.; Keeling, J.; Lovett, B. W., Efficient non-Markovian quantum dynamics using time-evolving matrix product operators. *Nature Communications* **2018**, 9, 3322.
21. Sato, Y., A scalable algorithm of numerical real-time path integral for quantum dissipative systems. *J. Chem. Phys.* **2019**, 150, 224108.
22. Wang, H., Basis set approach to the quantum dissipative dynamics: Application of the multiconfiguration time-dependent Hartree method to the spin-boson problem. *J. Chem. Phys.* **2000**, 113, 9948-9956.
23. Ishizaki, A.; Tanimura, Y., Quantum dynamics of system strongly coupled to low-temperature colored noise bath: Reduced hierarchy equations approach. *J. Phys. Soc. Jpn.* **2005**, 74, 3131-3134.
24. Makri, N., The linear response approximation and its lowest order corrections: an influence functional approach. *J. Phys. Chem.* **1999**, 103, 2823-2829.

25. Ehrenfest, P., Bemerkung über die angenäherte Gültigkeit der klassischen Mechanik innerhalb der Quantenmechanik. *Z. Phys.* **1927**, 45, 455-457.
26. Tully, J. C.; Preston, R. K., Trajectory surface hopping approach to nonadiabatic molecular collisions: the reaction of H+ with D2. *J. Chem. Phys.* **1971**, 55, 562-572.
27. Tully, J. C., Molecular dynamics with electronic transitions. *J. Chem. Phys.* **1990**, 93, 1061-1071.
28. Meyer, H.-D.; Miller, W. H., A classical analog for electronic degrees of freedom in nonadiabatic collision processes. *J. Chem. Phys.* **1979**, 70, 3214-3223.
29. Stock, G.; Thoss, M., Semiclassical description of nonadiabatic quantum dynamics. *Phys. Rev. Lett.* **1997**, 78, 578-581.
30. Wang, H.; Sun, X.; Miller, W. H., Semiclassical approximations for the calculation of thermal rate constants for chemical reactions in complex molecular systems. *J. Chem. Phys.* **1998**, 108, 9726-9736.
31. Donoso, A.; Martens, C. C., Simulation of coherent nonadiabatic dynamics using classical trajectories. *J. Phys. Chem. A* **1998**, 102, 4291.
32. Kapral, R.; Ciccotti, G., Mixed quantum-classical dynamics. *J. Chem. Phys.* **1999**, 110, 8919-8929.
33. Mac Kernan, D.; Ciccotti, G.; Kapral, R., Sequential short-time propagation of quantum-classical dynamics. *J. Phys. Cond. Matt.* **2002**, 14, 9069-9076.
34. Mac Kernan, D.; Ciccotti, G.; Kapral, R., Trotter based simulation of quantum-classical dynamics. *j . Phys. Chem. B* **2008**, 114.
35. Lambert, R.; Makri, N., Quantum-classical path integral: Classical memory and weak quantum nonlocality. *J. Chem. Phys.* **2012**, 137, 22A552.
36. Lambert, R.; Makri, N., Quantum-classical path integral: Numerical formulation. *J. Chem. Phys.* **2012**, 137, 22A553.
37. Makri, N., Quantum-classical path integral: A rigorous approach to condensed phase dynamics. *International Journal of Quantum Chemistry* **2015**, 115, 1209-1214.
38. Walters, P. L.; Makri, N., Quantum-classical path integral simulation of the ferrocene-ferrocenium charge transfer in liquid hexane. *J. Phys. Chem. Lett.* **2015**, 6, 4959-4965.
39. Makri, N., Modular path integral methodology for real-time quantum dynamics. *J. Chem. Phys.* **2018**, 149, 214108.
40. Makri, N., Modular path integral: Quantum dynamics via sequential necklace linking. *J. Chem. Phys.* **2018**, 148, 101101.
41. Kundu, S.; Makri, N., Modular path integral for discrete systems with non-diagonal couplings. *J. Chem. Phys.* **2019**, 151, 074110.
42. Feynman, R. P., Space-time approach to non-relativistic quantum mechanics. *Rev. Mod. Phys.* **1948**, 20, 367-387.
43. Feynman, R. P.; F. L. Vernon, J., The theory of a general quantum system interacting with a linear dissipative system. *Ann. Phys.* **1963**, 24, 118-173.
44. Makri, N., Blip decomposition of the path integral: Exponential acceleration of real-time calculations for quantum dissipative systems. *J. Chem. Phys.* **2014**, 141, 134117.
45. Makri, N., Iterative blip-summed path integral for quantum dynamics in strongly dissipative environments. *J. Chem. Phys.* **2017**, 146, 134101.
46. Lambert, R.; Makri, N., Memory path propagator matrix for long-time dissipative charge transport dynamics. *Mol. Phys.* **2012**, 110, 1967-1975.
47. Makri, N., Exploiting classical decoherence in dissipative quantum dynamics: Memory, phonon emission, and the blip sum. *Chem. Phys. Lett.* **2014**, 593, 93-103.
48. Walters, P. L.; Makri, N., Iterative quantum-classical path integral with dynamically consistent state hopping. *J. Chem. Phys.* **2016**, 144, 044108.
49. Banerjee, T.; Makri, N., Quantum-classical path integral with self-consistent solvent-driven propagators. *J. Phys. Chem.* **2013**, 117, 13357-13366.
50. Nakajima, S., On quantum theory of transport phenomena. *Prog. Theor. Phys* **1958**, 20, 948.

51. Zwanzig, R., Ensemble method in the theory of irreversibility. *J. Chem. Phys.* **1960**, 33, 1338-1341.
52. Redfield, A. G., On the theory of relaxation processes. *IBM Journal of Research and Development* **1957**, 1, 19-31.
53. Shi, Q.; Geva, E., A new approach to calculating the memory kernel in the generalized quantum master equation for an arbitrary system-bath coupling. *J. Chem. Phys.* **2003**, 119, 12063.
54. Mori, H., *Prog. Theor. Phys.* **1965**, 33, 423.
55. Montoya-Castillo, A.; Reichman, D. R., Approximate but accurate quantum dynamics from the Mori formalism: I. Nonequilibrium dynamics. *J. Chem. Phys.* **2016**, 144, 184104.
56. Kelly, A.; Montoya-Castillo, A.; Wang, L.; Markland, T. E., Generalized quantum master equations in and out of equilibrium: When can one win? *J. Chem. Phys.* **2016**, 144, 184105.
57. Kidon, L.; Wang, H.; Thoss, M.; Rabani, E., On the memory kernel and the reduced system propagator. *J. Chem. Phys.* **2018**, 149, 104105.
58. Mulvihill, E.; Gao, X.; Liu, Y.; Schubert, A.; Dunietz, B. D.; Geva, E., Combining the mapping Hamiltonian linearized semiclassical approach with the generalized quantum master equation to simulate electronically nonadiabatic molecular dynamics. *J. Chem. Phys.* **2019**, 151, 074103.
59. Pfalzgraff, W. C.; Kelly, A.; Markland, T. E., Nonadiabatic dynamics in atomistic environments: Harnessing quantum-classical theory with generalized quantum master equations. *J. Phys. Chem. Lett.* **2015**, 6, 4743−4748.
60. Kelly, A.; Brackbill, N.; Markland, T. E., Accurate nonadiabatic quantum dynamics on the cheap: Making the most of mean field theory with master equations. *J. Chem. Phys.* **2015**, 142, 094110.
61. Kelly, A.; Markland, T. E., Efficient and accurate surface hopping for long time nonadiabatic quantum dynamics. *J. Chem. Phys.* **2013**, 139, 014104.
62. Cohen, G.; Rabani, E., Memory effects in nonequilibrium quantum impurity models. *Phys. Rev. B* **2011**, 84, 075150.
63. Cohen, G.; Gull, E.; Reichman, D. R.; Millis, A. J.; Rabani, E., Numerically exact long-time magnetization dynamics at the nonequilibrium Kondo crossover of the Anderson impurity model. *Phys. Rev B* **2013**, 87, 195108.
64. Mulvihill, E.; Schubert , A.; Sun, X.; Dunietz, B. D.; Geva, E., A modified approach for simulating electronically nonadiabatic dynamics via the generalized quantum master equation. *J. Chem. Phys.* **2019**, 150, 034101.
65. Pfalzgraff, W. C.; Montoya-Castillo, A.; Kelly, A.; Markland, T. E., Efficient construction of generalized master equation memory kernels for multi-state systems from nonadiabatic quantum-classical dynamics. *The Journal of Chemical Physics* **2019**, 150, 244109.
66. Caldeira, A. O.; Leggett, A. J., Path integral approach to quantum Brownian motion. *Physica A* **1983**, 121, 587-616.
67. Walters, P. L.; Banerjee, T.; Makri, N., On iterative path integral calculations for a system interacting with a shifted dissipative bath. *J. Chem. Phys.* **2015**, 143, 074112.
68. Allen, T. C.; Walters, P. L.; Makri, N., Direct computation of influence functional coefficients from numerical correlation functions. *J. Chem. Theory and Comput.* **2016**, 12, 4169-4177.
69. Echave, J.; Clary, D. C., Potential optimized discrete variable representation. *J. Chem. Phys.* **1992**, 190, 225-230.
70. Topaler, M.; Makri, N., System-specific discrete variable representations for path integral calculations with quasi-adiabatic propagators. *Chem. Phys. Lett.* **1993**, 210, 448.
71. Thompson, K.; Makri, N., Influence functionals with semiclassical propagators in combined forward-backward time. *J. Chem. Phys.* **1999**, 110, 1343-1353.
72. Makri, N.; Thompson, K., Semiclassical influence functionals for quantum systems in anharmonic environments. *Chem. Phys. Lett.* **1998**, 291, 101-109.
73. Shi, Q.; Geva, E., A derivation of the mixed quantum-classical Liouville equation from the influence functional formalism. *J. Chem. Phys.* **2004**, 121, 3393-3404.
74. Wigner, E. J., Calculation of the Rate of Elementary Association Reactions. *Chem. Phys.* **1937**, 5, 720.

75. Shi, Q.; Geva, E., Semiclassical theory of vibrational energy relaxation in the condensed phase. *J. Phys. Chem. A* **2003**, 107, 9059-9069.
76. Poulsen, J. A.; Nyman, G.; Rossky, P. J., Practical evaluation of condensed phase quantum correlation functions: A Feynman--Kleinert variational linearized path integral method. *J. Chem. Phys.* **2003**, 119, 12179-12193.
77. Liu, J.; Miller, W. H., Using the thermal Gaussian approximation for the Boltzmann operator in semiclassical initial value time correlation functions. *The Journal of Chemical Physics* **2006**, 125, 224104.
78. Shao, J.; Pollak, E., A new time evolving Gaussian series representation of the imaginary time propagator. *J. Chem. Phys.* **2006**, 125, 133502.
79. Bose, A.; Makri, N., Evaluation of the Wigner distribution via classical adiabatic switching. *J. Chem. Phys.* **2015**, 143, 114114.
80. Bose, A.; Makri, N., Wigner Distribution by Adiabatic Switching in Normal Mode or Cartesian Coordinates and Molecular Applications. *J. Chem. Theory and Comput.* **2018**, 14, 5446–5458.
81. Bose, A.; Makri, N., Coherent state-based path integral methodology for computing the Wigner phase space distribution. *J. Phys. Chem. A* **2019**, 123, 4284-4294.
82. Makri, N., Dynamics of reduced density matrices: classical memory vs. quantum nonlocality. *J. Chem. Phys.* **1998**, 109, 2994-2998.
83. Walters, P. L.; Allen, T. C.; Makri, N., Direct determination of harmonic bath parameters from molecular dynamics simulations. *J. Comput. Chem.* **2017**, 38, 110-115.
84. Metropolis, N.; Rosenbluth, A. W.; Rosenbluth, M. N.; Teller, H.; Teller, E., Equation of state calculations by fast computing machines. *J. Chem. Phys.* **1953**, 21, 1087-1092.
85. Liang Zhang, M.-L.; Ka, B. J.; Geva, E., Nonequilibrium quantum dynamics in the condensed phase via the generalized quantum master equation *J. Chem. Phys.* **2006**, 125, 044106.
86. Onuchic, J. N.; Beratan, D. N.; Winkler, J. R.; Gray, H. B., Pathway analysis of protein electron transfer reactions. *Ann. Rev. Biophys. Biom. Struc.* **1992**, 21, 349.
87. Priyadarshy, S.; Risser, S. M.; Beratan, D. N., DNA is not a molecular wire: Protein-like electron-transfer predicted for an extended π-electron system. *J. Phys. Chem.* **1996**, 100.
88. Hedison, T. M.; Hay, S.; Scrutton, N. S., Real-time analysis of conformational control in electron transfer reactions of human cytochrome P450 reductase with cytochrome c. *FEBS J.* **2015**, 282, 4357–4375.

TOC Graphic

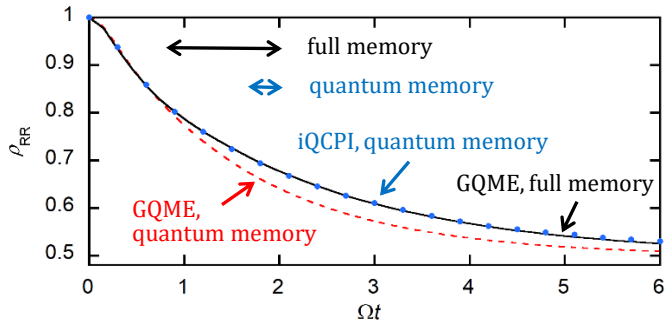
full memory
quantum memory
iQCPI, quantum memory
GQME, full memory
GQME,
quantum memory
ρ_{RR}
Ωt
1
0.9
0.8
0.7
0.6
0.5
0
1
2
3
4
5
6